GEOPHYSICS, VOL. 70, NO. 6 (NOVEMBER-DECEMBER 2005); P. D65–D75, 8 FIGS.
10.1190/1.2122411

First-order ray tracing for qP waves in inhomogeneous, weakly anisotropic media

Ivan Pšenčík[1] and Véronique Farra[2]

ABSTRACT

We propose approximate ray-tracing equations for qP-waves propagating in smooth, inhomogeneous, weakly anisotropic media. For their derivation, we use perturbation theory, in which deviations of anisotropy from isotropy are considered to be the first-order quantities. The proposed ray-tracing equations and corresponding traveltimes are of the first order. Accuracy of the traveltimes can be increased by calculating a second-order correction along first-order rays.

The first-order ray-tracing equations for qP-waves propagating in a general weakly anisotropic medium depend on only 15 weak-anisotropy parameters (generalization of Thomsen's parameters). The equations are thus considerably simpler than the exact ray-tracing equations. For higher-symmetry anisotropic media the equations differ only slightly from equations for isotropic media. They can thus substitute for the traditional isotropic ray tracers used in seismic processing. For vanishing anisotropy, the first-order ray-tracing equations reduce to standard, exact ray-tracing equations for isotropic media. Numerical tests for configuration and models used in seismic prospecting indicate negligible dependence of accuracy of calculated traveltimes on inhomogeneity of the medium. For anisotropy of about 8%, considered in the examples presented, the relative errors of the traveltimes, including the second-order correction, are well under 0.05%; for anisotropy of about 20%, they do not exceed 0.3%.

INTRODUCTION

Ray-tracing procedures represent the basis of many seismic processing techniques, such as prestack Kirchhoff depth migration or amplitude versus offset (AVO). Since studied media are often anisotropic and specifically weakly anisotropic, development of ray-tracing procedures for such kinds of media is desirable (see, e.g., Daley et al., 1999). The most natural specification of weakly anisotropic media is by the weak-anisotropy parameters, which represent a generalization of Thomsen's (1986) parameters for transversely isotropic media to weakly anisotropic media of arbitrary symmetry [see, e.g., Farra and Pšenčík (2003)]. Individual seismic waves depend only on selected subsets of these parameters. Specifically, qP-wave propagation is controlled by 15 weak-anisotropy parameters, which include all 21 elastic moduli but with some of them in combination with others. Standard ray-tracing equations for anisotropic media do not reflect this fact. Standard ray-tracing equations are the same for all three waves propagating in anisotropic media. The wave type must be specified by the initial (at the source or at an interface) conditions. Although notation can act as a mask, the right-hand sides of the standard ray-tracing equations are quite complicated. They contain up to 81 terms consisting of individual elastic parameters. Very often, however, many of these terms are zero or are mutually dependent. Thus, calculating the right-hand sides of ray-tracing equations requires many unnecessary operations, which may increase numerical errors.

We use perturbation theory, in which deviations of anisotropy from isotropy are considered to be of the first order, and we derive approximate ray-tracing equations for qP-waves, which depend on the above-mentioned 15 qP-wave weak-anisotropy parameters and which can be used for tracing qP-wave rays only. Similar approximate ray-tracing equations can be derived for qS-waves (see Farra, 2005). The derivation of ray-tracing equations for qP-waves is, of course, simpler because it is not complicated by the possibility of encountering singularities. The approximate ray-tracing equations are derived from the exact ones, in which the exact eigenvalue of the Christoffel matrix is substituted by its first-order approximation. We therefore speak about first-order ray tracing (FORT). FORT differs from other perturbation approaches for tracing rays [see, e.g., Farra (1989) and Nowack and Pšenčík (1991)] because it does not require calculation of reference rays in a reference medium. FORT provides directly

Manuscript received by the Editor November 3, 2004; revised manuscript received February 24, 2005; published online October 12, 2005.
[1]Geophysical Institute, Academy of Sciences of the Czech Republic, 141 31 Prague 4, Czech Republic. E-mail: ip@ig.cas.cz.
[2]Institut de Physique du Globe de Paris, Département de Sismologie, 4 Place Jussieu, 75252 Paris Cedex 05, France. E-mail: farra@ipgp.jussieu.fr.

the first-order rays and the first-order traveltimes along them. To increase accuracy of traveltimes, a simple second-order traveltime correction based on numerical quadratures along the FORT ray can be used.

The FORT method is very simple and transparent. It represents a generalization of isotropic ray tracing to which it reduces for isotropic media. It can thus be used as a substitute for isotropic ray tracers in routine applications such as Kirchhoff depth migration (Portugal et al., 2003), based on ray tracing or wavefront construction (see Vinje et al., 1993).

After a brief review of standard (exact) ray-tracing equations in the following section, we devote a section to the derivation of the FORT equations and present specifications for most common types of anisotropic media of higher symmetry in the section that follows. Afterward, the second-order traveltime correction, which can be evaluated by a simple integration along a first-order ray, is derived. The following section contains a brief description of how to derive the first-order dynamic ray-tracing (FODRT) equations. The final sections are devoted to numerical examples illustrating the accuracy of the proposed approach and to our conclusions. Appendix A contains definitions of the weak-anisotropy parameters and explicit expressions for the elements B_{13}, B_{23}, and B_{33} of the weak-anisotropy matrix B_{mn}.

In the following, component notation is used. Einstein summation convention is used for the repeated subscripts. Subscripts behind a comma denote differentiation with respect to the corresponding spatial coordinates.

FORMULAS FOR EXACT RAY TRACING

We start from the formulas for exact ray tracing in inhomogeneous anisotropic media:

$$\frac{dx_i}{d\tau} = \frac{1}{2}\frac{\partial G}{\partial p_i}, \qquad \frac{dp_i}{d\tau} = -\frac{1}{2}\frac{\partial G}{\partial x_i}. \tag{1a,b}$$

(See, e.g., Červený, 2001.) Here, x_i denote coordinates of the trajectory of the ray and p_i denote components of the slowness vector at corresponding points of the ray, $p_i = n_i/c$. The vector n_i is the unit normal to the wavefront (the unit vector parallel to the slowness vector p_i), and $c = c(x_m, n_m)$ is the phase velocity. Note that equation 1a represents the ray-velocity vector. The variable τ in equation 1a and b, which has the physical meaning of propagation time, is a parameter along the ray. The symbol $G = G(x_m, p_m)$ denotes one of the three eigenvalues of the generalized Christoffel matrix:

$$\Gamma_{ik}(x_m, p_m) = a_{ijkl}(x_m) p_j\ p_l. \tag{2}$$

The matrix $\Gamma_{ik}(x_m, p_m)$ is called the generalized Christoffel matrix, in contrast to the standard Christoffel matrix $\Gamma_{ik}(x_m, n_m) = a_{ijkl}(x_m) n_j\ n_l$, in which the slowness vector p_m is substituted by the wave normal n_m. Here, a_{ijkl} is a tensor of density-normalized elastic moduli. At each point of a ray, the slowness vector determined from equation 1a,b must satisfy the eikonal equation

$$G(x_m, p_m) = \Gamma_{ik}(x_m, p_m) g_i\ g_k = 1. \tag{3}$$

The unit vectors g_m represent polarization vectors. They are identical to the eigenvectors of the generalized Christoffel matrix 2.

Using equations 2 and 3, we can rewrite ray-tracing system 1 as

$$\frac{dx_i}{d\tau} = a_{ijkl}\ p_l\ g_j\ g_k, \quad \frac{dp_i}{d\tau} = -\frac{1}{2} a_{njkl,i}\ p_j\ p_l\ g_n\ g_k. \tag{4a,b}$$

This ray-tracing system looks very simple, but in fact, the right-hand side of equation 4a consists of 27 terms and the right-hand side of equation 4b consists of 81 terms containing individual elastic moduli. In practical applications, many of these terms are zero or are mutually dependent. Thus, evaluation of the right-hand sides of equations 4 typically requires more operations than are needed.

Because the eigenvalue $G(x_m, p_m)$ of the generalized Christoffel matrix is a homogeneous function of the second degree in p_m (see, e.g., Červený, 2001, 22), and $p_m = p\ n_m = c^{-1}\ n_m$, we can write

$$G(x_m, p_m) = p^2 G(x_m, n_m) = c^{-2}(x_m, n_m) G(x_m, n_m). \tag{5}$$

Here, p is the slowness, $p^2 = p_k p_k = c^{-2}$. Combining equation 5 with the eikonal equation 3 and taking into account that the generalized Christoffel matrix $\Gamma_{ik}(x_m, p_m)$ is a homogeneous function of the second degree in p_m, we find that

$$c^2(x_m, n_m) = G(x_m, n_m) = \Gamma_{ik}(x_m, n_m) g_i g_k. \tag{6}$$

The initial conditions for the ray-tracing system 4 for $\tau = 0$ have the form

$$x_i(0) = x_i^0, \qquad p_i(0) = p_i^0, \tag{7}$$

where x_i^0 denote the coordinates of the initial point of the ray and p_i^0 denote the components of the slowness vector at the same point specified as $p_i^0 = n_i^0/c_0$. They must satisfy equation 3. The symbol c_0 denotes the phase velocity at the point x_i^0 in a given direction n_i^0. For the given n_i^0, the phase velocity c_0 can be determined from equation 6.

FIRST-ORDER RAY-TRACING FORMULAS FOR qP-WAVES

For the first set of FORT equations, we could use the expressions for the first-order ray-velocity vector derived by Pšenčík and Vavryčuk (2002) and Farra (2004). Here, however, we start from the ray-tracing equations 1, in which we substitute the exact eigenvalue by its first-order approximation for qP-waves. Farra (2001) and Farra and Pšenčík (2003) show that the first-order approximations $G^{(1)}$ and $c^{(1)}$ of $G(x_m, n_m)$ and of the phase velocity $c(x_m, n_m)$, respectively, satisfy an equation analogous to equation 6:

$$G^{(1)}(x_m, n_m) = \Gamma_{jk}(x_m, n_m) g_j^{(0)} g_k^{(0)} = c^{(1)2}(x_m, n_m), \tag{8}$$

where $g_m^{(0)} = n_m$. The symbol $g_m^{(0)}$ denotes zero-order approximation of the polarization vector. Because $G^{(1)}(x_m, n_m)$ and $\Gamma_{jk}(x_m, n_m)$ are homogeneous functions of the second degree

in n_m, we can write, similarly to equation 5,

$$G^{(1)}\big(x_m, p_m^{(1)}\big) = p^{(1)2}\, G^{(1)}(x_m, n_m) = (c^{(1)})^{-2}\, G^{(1)}(x_m, n_m), \tag{9}$$

where $p_m^{(1)} = n_m/c^{(1)}$ and $p^{(1)} = (c^{(1)})^{-1}$ are the first-order approximations of the slowness vector p_m in the direction n_m and of the slowness p, $p^{(1)2} = p_k^{(1)} p_k^{(1)}$. Thus, for the first-order approximation of the phase velocity, we can write

$$(c^{(1)})^{-2} = p_i^{(1)} p_i^{(1)}. \tag{10}$$

Comparing equations 8 and 9, and remembering that $g_m^{(0)} = n_m$, yields the first-order analog of the eikonal equation 3:

$$G^{(1)}\big(x_m, p_m^{(1)}\big) = \Gamma_{ik}\big(x_m, p_m^{(1)}\big) n_i n_k = 1. \tag{11}$$

By comparing equations 6 and 8, we can see that $c^{(1)}$ is a good approximation of c if the wave normal n_i is a good approximation of the polarization vector g_i. Because along longitudinal directions (directions in which the qP-wave polarization is strictly longitudinal) $c = c^{(1)}$ and $g_i = n_i$ (see Farra and Pšenčík, 2003), we can expect that in these directions and close to them, the first-order formulas will work especially well.

We now substitute $G^{(1)}$ as defined in equations 9 and 11 for the exact eigenvalue G in ray-tracing equations 1. Because we are going to deal with first-order quantities only, we omit subscripts indicating that the quantities are of the first order, returning to the original notation only when confusion could arise. Under this specification, the FORT system has formally exactly the same form as the ray-tracing system in equation 1. The FORT equations, however, generate only approximate (first-order) values of coordinates x_i and of slowness vectors p_i, different from the exact values generated by ray-tracing equations 1 with the exact eigenvalue G.

Because $G(x_m, p_m)$ is related to $G(x_m, n_m)$ (see equation 9), we concentrate first on the quantity $G(x_m, n_m)$. Combining equation 15 of Farra and Pšenčík (2003) and the last equation of set A4 in the same paper yields an explicit expression for $G(x_m, n_m)$:

$$\begin{aligned} G(x_m, n_m) &= c^2(x_m, n_m) \\ &= \alpha^2\big\{1 + 2\big(\epsilon_x n_1^2 + \epsilon_y n_2^2 + \epsilon_z n_3^2\big) \\ &\quad + 2\big(\eta_x n_2^2 n_3^2 + \eta_y n_3^2 n_1^2 + \eta_z n_1^2 n_2^2\big) \\ &\quad + 4\big[(\epsilon_{16} n_2 + \epsilon_{15} n_3) n_1^3 + (\epsilon_{24} n_3 + \epsilon_{26} n_1) n_2^3 \\ &\quad + (\epsilon_{35} n_1 + \epsilon_{34} n_2) n_3^3 \\ &\quad + (\chi_x n_1 + \chi_y n_2 + \chi_z n_3) n_1 n_2 n_3\big]\big\}, \end{aligned} \tag{12}$$

where

$$\eta_x = \delta_y - \epsilon_y - \epsilon_z, \quad \eta_y = \delta_x - \epsilon_x - \epsilon_z, \quad \eta_z = \delta_z - \epsilon_x - \epsilon_y. \tag{13}$$

The quantity α in equation 12 is a reference velocity used to define weak-anisotropy parameters (see equation A-1). We can easily show that equation 12 is independent of α (see equation A-5). The reference velocity α can thus be chosen as an arbitrary nonzero constant ($\alpha \neq 0$).

We can now insert equations 9 and 12 into equation 1 and derive explicit formulas. When doing so, we must carefully distinguish which quantities depend on spatial coordinates x_i and which depend on the components p_i of the slowness vector. In equation 9, the only spatially dependent quantities are the elastic moduli a_{ijkl}. All remaining quantities are functions of p_m. In the following derivations, we also use the relation $n_k = p^{-1} p_k$. The resulting FORT equations read

$$\begin{aligned} \frac{dx_1}{d\tau} &= \alpha^2 p_1 + 2\alpha^2 \epsilon_x p_1 + 2\alpha^2 (p_k p_k)^{-2}\big\{\big(p_2^2 + p_3^2\big) \\ &\quad \times \big(\eta_y p_3^2 + 2\chi_x p_2 p_3 + \eta_z p_2^2\big) p_1 + \big(p_2^2 + p_3^2 - p_1^2\big) \\ &\quad \times \big(\epsilon_{35} p_3^3 + \chi_z p_2 p_3^2 + \chi_y p_3 p_2^2 + \epsilon_{26} p_2^3\big) \\ &\quad + \big[p_1^2 + 3\big(p_2^2 + p_3^2\big)\big](\epsilon_{15} p_3 + \epsilon_{16} p_2) p_1^2 \\ &\quad - \big(2\epsilon_{34} p_3^2 + \eta_x p_2 p_3 + 2\epsilon_{24} p_2^2\big) p_1 p_2 p_3\big\}, \end{aligned} \tag{14a}$$

$$\begin{aligned} \frac{dx_2}{d\tau} &= \alpha^2 p_2 + 2\alpha^2 \epsilon_y p_2 + 2\alpha^2 (p_k p_k)^{-2}\big\{\big(p_1^2 + p_3^2\big) \\ &\quad \times \big(\eta_x p_3^2 + 2\chi_y p_1 p_3 + \eta_z p_1^2\big) p_2 + \big(p_1^2 + p_3^2 - p_2^2\big) \\ &\quad \times \big(\epsilon_{34} p_3^3 + \chi_z p_1 p_3^2 + \chi_x p_3 p_1^2 + \epsilon_{16} p_1^3\big) \\ &\quad + \big[3\big(p_1^2 + p_3^2\big) + p_2^2\big](\epsilon_{24} p_3 + \epsilon_{26} p_1) p_2^2 \\ &\quad - \big(2\epsilon_{35} p_3^2 + \eta_y p_1 p_3 + 2\epsilon_{15} p_1^2\big) p_1 p_2 p_3\big\}, \end{aligned} \tag{14b}$$

$$\begin{aligned} \frac{dx_3}{d\tau} &= \alpha^2 p_3 + 2\alpha^2 \epsilon_z p_3 + 2\alpha^2 (p_k p_k)^{-2}\big\{\big(p_1^2 + p_2^2\big) \\ &\quad \times \big(\eta_y p_1^2 + 2\chi_z p_1 p_2 + \eta_x p_2^2\big) p_3 + \big(p_1^2 + p_2^2 - p_3^2\big) \\ &\quad \times \big(\epsilon_{15} p_1^3 + \chi_x p_1^2 p_2 + \chi_y p_1 p_2^2 + \epsilon_{24} p_2^3\big) \\ &\quad + \big[3\big(p_1^2 + p_2^2\big) + p_3^2\big](\epsilon_{34} p_2 + \epsilon_{35} p_1) p_3^2 \\ &\quad - \big(2\epsilon_{16} p_1^2 + \eta_z p_1 p_2 + 2\epsilon_{26} p_2^2\big) p_1 p_2 p_3\big\}, \end{aligned} \tag{14c}$$

and

$$\begin{aligned} \frac{dp_i}{d\tau} &= -\alpha^2 (p_k p_k)^{-1}\big[2p_3^3(\epsilon_{34,i} p_2 + \epsilon_{35,i} p_1) \\ &\quad + p_3^2\big(\eta_{y,i} p_1^2 + \eta_{x,i} p_2^2 + 2\chi_{z,i} p_1 p_2\big) \\ &\quad + 2p_3\big(\chi_{x,i} p_1^2 p_2 + \chi_{y,i} p_1 p_2^2 + \epsilon_{15,i} p_1^3 + \epsilon_{24,i} p_2^3\big) \\ &\quad + (p_k p_k)\big(\epsilon_{x,i} p_1^2 + \epsilon_{y,i} p_2^2 + \epsilon_{z,i} p_3^2\big) + \eta_{z,i} p_1^2 p_2^2 \\ &\quad + 2\epsilon_{16,i} p_1^3 p_2 + 2\epsilon_{26,i} p_1 p_2^3\big]. \end{aligned} \tag{14d}$$

The symbols η_x, η_y, and η_z are defined in equation 13.

Equations 14 represent the FORT equations for 3D inhomogeneous, weakly anisotropic media of arbitrary symmetry in the explicit form. The right-hand sides contain a maximum 16 terms in contrast to 27 and 81 in the case of exact ray tracing. Moreover, in the FORT equations 14, we can see immediately how each of the 15 weak-anisotropy parameters specifying the medium affects the ray. At each point of the ray, the

slowness vector p_i determined from equation 14d satisfies the first-order eikonal equation 11.

The initial conditions at the source for $\tau = 0$ have formally the same form as in equation 7:

$$x_i(0) = x_i^0, \qquad p_i(0) = p_i^0. \tag{15}$$

Here, x_i^0 are the coordinates of the source point and p_i^0 are the components of the slowness vector in the first-order approximation, specified as $p_i^0 = n_i^0/c_0$. The symbol c_0 denotes the first-order approximation of the phase velocity in the direction n_i^0 at the point x_i^0. The phase velocity is given by the square root of the expression given in equation 12 specified for x_i^0 and n_i^0.

Because $G(x_m, n_m)$ in equation 12 is independent of α, equations 14 are also independent of α. The symbol α appears in equation 14 only because the weak-anisotropy parameters in equation A-1 are used. If density-normalized elastic moduli $A_{\alpha\beta}$ (in the Voigt notation) are used instead of the weak-anisotropy parameters, the symbol α disappears from the FORT equations (see FORT equations 25 for VTI media).

FORT EQUATIONS FOR qP-WAVES IN ANISOTROPIC MEDIA OF HIGHER SYMMETRY

The FORT equations 14 simplify considerably in media with higher symmetry anisotropy. We present FORT equations for some of the most common types of anisotropic media.

FORT equations for orthorhombic media

For an orthorhombic medium that has planes of symmetry coinciding with the coordinate planes,

$$\chi_x = \chi_y = \chi_z = \epsilon_{15} = \epsilon_{16} = \epsilon_{24} = \epsilon_{26} = \epsilon_{34} = \epsilon_{35} = 0. \tag{16}$$

Taking this into account in equations 14, we arrive at the FORT equations for 3D inhomogeneous orthorhombic media:

$$\frac{dx_1}{d\tau} = \alpha^2 p_1\big\{1 + 2\epsilon_x + 2(p_k p_k)^{-2}\big[\big(p_2^2 + p_3^2\big) \times \big(\eta_y p_3^2 + \eta_z p_2^2\big) - \eta_x p_2^2 p_3^2\big]\big\}, \tag{17a}$$

$$\frac{dx_2}{d\tau} = \alpha^2 p_2\big\{1 + 2\epsilon_y + 2(p_k p_k)^{-2}\big[\big(p_1^2 + p_3^2\big) \times \big(\eta_x p_3^2 + \eta_z p_1^2\big) - \eta_y p_1^2 p_3^2\big]\big\}, \tag{17b}$$

$$\frac{dx_3}{d\tau} = \alpha^2 p_3\big\{1 + 2\epsilon_z + 2(p_k p_k)^{-2}\big[\big(p_1^2 + p_2^2\big) \times \big(\eta_y p_1^2 + \eta_x p_2^2\big) - \eta_z p_1^2 p_2^2\big]\big\}, \tag{17c}$$

and

$$\frac{dp_i}{d\tau} = -\alpha^2 (p_k p_k)^{-1}\big[\eta_{y,i} p_1^2 p_3^2 + \eta_{x,i} p_2^2 p_3^2 + \eta_{z,i} p_1^2 p_2^2 + (p_k p_k)\big(\epsilon_{x,i} p_1^2 + \epsilon_{y,i} p_2^2 + \epsilon_{z,i} p_3^2\big)\big]. \tag{17d}$$

The initial conditions are given again by equation 15. The formula 12 for the square of the first-order phase velocity reduces in this case to

$$c^2(x_m, n_m) = \alpha^2\big[1 + 2\big(\epsilon_x n_1^2 + \epsilon_y n_2^2 + \epsilon_z n_3^2 + \eta_x n_2^2 n_3^2 + \eta_y n_3^2 n_1^2 + \eta_z n_1^2 n_2^2\big)\big]. \tag{18}$$

FORT equations for HTI media

In the case of transverse isotropy with a horizontal axis of symmetry (HTI) oriented along the x_1-axis, we have, in addition to conditions 16,

$$\epsilon_y = \epsilon_z = \tfrac{1}{2}\delta_y, \quad \delta_x = \delta_z, \quad \eta_y = \eta_z, \quad \eta_x = 0. \tag{19}$$

Inserting this into equations 17, we get the FORT equations for 3D inhomogeneous HTI media, which have the form:

$$\frac{dx_1}{d\tau} = \alpha^2 p_1\big[1 + 2\epsilon_x + 2(p_k p_k)^{-2}\eta_z\big(p_2^2 + p_3^2\big)^2\big], \tag{20a}$$

$$\frac{dx_2}{d\tau} = \alpha^2 p_2\big[1 + 2\epsilon_z + 2(p_k p_k)^{-2}\eta_z p_1^4\big], \tag{20b}$$

$$\frac{dx_3}{d\tau} = \alpha^2 p_3\big[1 + 2\epsilon_z + 2(p_k p_k)^{-2}\eta_z p_1^4\big], \tag{20c}$$

and

$$\frac{dp_i}{d\tau} = -\alpha^2 (p_k p_k)^{-1}\big\{\eta_{z,i}\big(p_2^2 + p_3^2\big)p_1^2 + (p_k p_k) \times \big[\epsilon_{x,i} p_1^2 + \epsilon_{z,i}\big(p_2^2 + p_3^2\big)\big]\big\}. \tag{20d}$$

The initial conditions are given by equation 15. The square of the first-order phase velocity now has the form

$$c^2(x_m, n_m) = \alpha^2\big\{1 + 2\big[\eta_z n_1^2\big(1 - n_1^2\big) + \epsilon_x n_1^2 + \epsilon_z\big(1 - n_1^2\big)\big]\big\}. \tag{21}$$

FORT equations for VTI media

In the case of transverse isotropy with a vertical axis of symmetry (VTI) oriented along the x_3-axis, we have, in addition to conditions 16,

$$\epsilon_x = \epsilon_y = \tfrac{1}{2}\delta_z, \quad \delta_x = \delta_y, \quad \eta_x = \eta_y, \quad \eta_z = 0. \tag{22}$$

Inserting this into equations 17, we get the FORT equations for 3D inhomogeneous VTI media, which have the following simple form:

$$\frac{dx_1}{d\tau} = \alpha^2 p_1\big[1 + 2\epsilon_x + 2(p_k p_k)^{-2}\eta_x p_3^4\big], \tag{23a}$$

$$\frac{dx_2}{d\tau} = \alpha^2 p_2\big[1 + 2\epsilon_x + 2(p_k p_k)^{-2}\eta_x p_3^4\big], \tag{23b}$$

$$\frac{dx_3}{d\tau} = \alpha^2 p_3\big[1 + 2\epsilon_z + 2(p_k p_k)^{-2}\eta_x\big(p_1^2 + p_2^2\big)^2\big], \tag{23c}$$

and

$$\frac{dp_i}{d\tau} = -\alpha^2 (p_k p_k)^{-1}\big\{\eta_{x,i}\big(p_1^2 + p_2^2\big)p_3^2 + (p_k p_k)\big[\epsilon_{x,i}\big(p_1^2 + p_2^2\big) + \epsilon_{z,i} p_3^2\big]\big\}. \tag{23d}$$

The initial conditions are given by equation 15. The square of the phase velocity is given by

$$c^2(x_m, n_m) = \alpha^2\big\{1 + 2\big[\eta_x n_3^2\big(1 - n_3^2\big) + \epsilon_z n_3^2 + \epsilon_x\big(1 - n_3^2\big)\big]\big\}. \tag{24}$$

If density-normalized elastic moduli in Voigt notation $A_{\alpha\beta}$ are used instead of weak-anisotropy parameters, the FORT equations 23 can be rewritten in the following form:

$$\frac{dx_1}{d\tau} = p_1\left[A_{11} + (p_k p_k)^{-2} E_x p_3^4\right], \tag{25a}$$

$$\frac{dx_2}{d\tau} = p_2\left[A_{11} + (p_k p_k)^{-2} E_x p_3^4\right], \tag{25b}$$

$$\frac{dx_3}{d\tau} = p_3\left[A_{33} + (p_k p_k)^{-2} E_x \left(p_1^2 + p_2^2\right)^2\right], \tag{25c}$$

and

$$\frac{dp_i}{d\tau} = -\frac{1}{2}(p_k p_k)^{-1}\left\{E_{x,i}\left(p_1^2 + p_2^2\right)p_3^2 + (p_k p_k)\left[A_{11,i}\left(p_1^2 + p_2^2\right) + A_{33,i}p_3^2\right]\right\}. \tag{25d}$$

When specifying equations 25, relations 22 are taken into account. In equations 25, $E_x = E_y = 2A_{13} + 4A_{55} - A_{11} - A_{33}$ (see equation A-6). Note that FORT equations 25 do not contain the reference velocity α used for the definition of the weak-anisotropy parameters.

FORT equations for isotropic media

In isotropic media we have, in addition to conditions 16,

$$\epsilon_x = \epsilon_y = \epsilon_z = \tfrac{1}{2}\delta_x = \tfrac{1}{2}\delta_y = \tfrac{1}{2}\delta_z, \quad \eta_x = \eta_y = \eta_z = 0. \tag{26}$$

The FORT equations then have the following form:

$$\frac{dx_i}{d\tau} = \alpha^2 p_i(1 + 2\epsilon_x), \qquad \frac{dp_i}{d\tau} = -\alpha^2(p_k p_k)\epsilon_{x,i}. \tag{27a,b}$$

Using the expression for ϵ_x from equation A-1, we find that equations 27 represent exact ray-tracing equations for a 3D inhomogeneous isotropic medium with a velocity $\sqrt{A_{11}}$. The FORT method can thus be used universally for isotropic as well as weakly anisotropic media. In isotropic media it yields exact rays; in anisotropic media, their first-order approximation.

SECOND-ORDER TRAVELTIME PERTURBATION

Farra and Le Bégat (1995) and Červený (2001) show that an approximate traveltime τ calculated along an approximate ray Ω_0, specified by an approximate eigenvalue $G(x_m, p_m)$ of the generalized Christoffel matrix can be improved to the first order by using the correction $\Delta\tau$:

$$\Delta\tau = -\frac{1}{2}\int_{\Omega_0} \Delta G(x_m, p_m) d\tau. \tag{28}$$

Equation 28 follows, for example, from equations 3.9.6 and 3.9.11 of Červený (2001). Here, Ω_0 denotes the approximate reference ray and x_m and p_m are coordinates and components of the slowness vector along it. The symbol ΔG denotes the difference between the exact eigenvalue and its approximation along Ω_0.

We can apply equation 28 to the FORT method by taking a FORT ray to be the ray Ω_0. From now to the end of this section, we use superscripts over the eigenvalue G, traveltime τ, and phase velocity c to indicate their approximation order. The coordinates x_m and slowness vectors p_m along Ω_0, which are first-order quantities, are left without superscripts. In the FORT method, the above-mentioned approximate traveltime τ is the first-order traveltime $\tau^{(1)}$ calculated along a FORT ray specified by $G^{(1)}(x_m, p_m)$. Note that the traveltime $\tau^{(1)}$ is obtained automatically by solving any of the FORT systems presented in this paper. For $\tau^{(1)}$ calculated between two points of the ray Ω_0, we can write

$$\tau^{(1)} = \int_{\Omega_0} G^{(1)}(x_m, p_m) d\tau = \int_{\Omega_0} d\tau. \tag{29}$$

In equation 29, we take into account that $G^{(1)}(x_m, p_m) = 1$ along Ω_0 (see equation 11). For the evaluation of ΔG, we need an estimate of exact G. Because $\Delta G = G - G^{(1)}$, it makes no sense to approximate G by $G^{(1)}$ since it would bring no correction to the traveltime. Therefore, we approximate $G(x_m, p_m)$ by its second-order approximation $G^{(2)}(x_m, p_m)$ along the ray Ω_0.

Farra and Pšenčík (2003) offer an expression for $G^{(2)}(x_m, n_m)$. From their equation 14, one gets

$$G^{(2)}(x_m, n_m) = G^{(1)}(x_m, n_m) + \frac{B_{13}^2(x_m, n_m) + B_{23}^2(x_m, n_m)}{V_P^2 - V_S^2}. \tag{30}$$

Because $G^{(1)}(x_m, n_m)$ and $G^{(2)}(x_m, n_m)$ are homogeneous functions of the second degree with respect to n_m, we can rewrite equation 30 in the following form:

$$G^{(2)}(x_m, p_m) = 1 + [c^{(1)}(x_m, n_m)]^{-2} \times \frac{B_{13}^2(x_m, n_m) + B_{23}^2(x_m, n_m)}{V_P^2 - V_S^2}, \tag{31}$$

where we again take equation 11 into account. In equation 31, V_P and V_S are P- and S-wave velocities of a reference isotropic medium closely approximating the studied weakly anisotropic medium. The velocity V_P has nothing to do with the velocity α used for the definition of the weak-anisotropy parameters (see equations A-1). Thus, V_P can be chosen as different from α. The quantities B_{13} and B_{23} are elements of the matrix

$$B_{ij}(x_m, n_m) = \Gamma_{kl}(x_m, n_m)\mathbf{e}_k^i \mathbf{e}_l^j \tag{32}$$

(see Farra and Pšenčík, 2003). For elements B_{13}, B_{23}, and B_{33}, see Appendix A. The symbols e_m^j denote components of three mutually perpendicular unit vectors $\mathbf{e}_m^1$, $\mathbf{e}_m^2$, and $\mathbf{e}_m^3$. The vector $\mathbf{e}_m^3$ is chosen so that $\mathbf{e}_m^3 = n_m$. The vectors $\mathbf{e}_m^1$ and $\mathbf{e}_m^2$ are situated in the plane perpendicular to $\mathbf{e}_m^3$. While B_{13} and B_{23} appear in the expression for $G^{(2)}$, $G^{(1)} = B_{33}$ (see Farra and Pšenčík, 2003). As illustrated by B_{33} in equation A-5, the matrix B_{mn} is independent of the choice of the reference velocity α. It can also be shown that B_{33} as well as $B_{13}^2 + B_{23}^2$ are independent of choice of vectors $\mathbf{e}_i^1$ and $\mathbf{e}_i^2$ in the plane perpendicular to $\mathbf{e}_i^3$. Any pair of unit, mutually perpendicular vectors $\mathbf{e}_i^1$ and $\mathbf{e}_i^2$ situated in the plane perpendicular to $\mathbf{e}_i^3$ gives the same B_{33} and $B_{13}^2 + B_{23}^2$. In equation 31 we can thus use equation A-2, which gives explicit expressions for the

elements B_{13}, B_{23}, and B_{33} when the vector $\mathbf{e}_m^2$ is chosen to be horizontal.

We can now return to equation 28. Inserting equation 31 into it, we get

$$\begin{aligned}\Delta\tau &= \tau^{(2)} - \tau^{(1)} \\ &= -\frac{1}{2}\int_{\Omega_0} [c^{(1)}(x_m, n_m)]^{-2} \\ &\quad \times \frac{B_{13}^2(x_m, n_m) + B_{23}^2(x_m, n_m)}{V_P^2 - V_S^2} d\tau. \end{aligned} \tag{33}$$

This is the second-order correction of the first-order traveltime $\tau^{(1)}$. It can be easily evaluated by numerical quadratures along the FORT ray; $c^{(1)}$ can be evaluated using equation 10.

It is easy to see that correction equation 33 is always negative or zero. Also note that the integrand of correction 33 is proportional to the factor used in the first-order approximation of the polarization vector (see equation 13 of Farra and Pšenčík, 2003). Thus, the second-order traveltime correction is related to the first-order corrections of the polarization vectors along a FORT ray.

FIRST-ORDER DYNAMIC RAY-TRACING FORMULAS

First-order dynamic ray tracing (FODRT) can be developed in the same way as exact dynamic ray tracing [see, e.g., Gajewski and Pšenčík (1990) and Červený (2001)]. If we denote a parameter specifying the FORT ray (e.g., one of its initial angles) by γ, we can introduce the following important quantities:

$$X_j = \left(\frac{\partial x_j}{\partial \gamma}\right)_{\tau=const}, \quad Y_j = \left(\frac{\partial p_j}{\partial \gamma}\right)_{\tau=const}. \tag{34}$$

The quantities X_j and Y_j describe variations along the wavefront of coordinates x_i and of the components p_i of the slowness vector, which result from variations of the parameter γ. The values of X_j and Y_j can be found from a system of linear differential equations obtained by the differentiation of the FORT equations with respect to γ:

$$\frac{dX_i}{d\tau} = \frac{1}{2}\left[\frac{\partial^2 G(x_m, p_m)}{\partial p_i \partial x_j} X_j + \frac{\partial^2 G(x_m, p_m)}{\partial p_i \partial p_j} Y_j\right], \tag{35a}$$

$$\frac{dY_i}{d\tau} = -\frac{1}{2}\left[\frac{\partial^2 G(x_m, p_m)}{\partial x_i \partial x_j} X_j + \frac{\partial^2 G(x_m, p_m)}{\partial x_i \partial p_j} Y_j\right]. \tag{35b}$$

The second derivatives of the first-order eigenvalue $G(x_m, p_m)$ of the Christoffel matrix in equations 35 can be obtained in the same way as the first derivatives necessary for evaluating the right-hand sides of the FORT equations were obtained. The FODRT solution has equally broad potential applications as its exact counterpart, dynamic ray tracing (see, e.g., Červený 2001).

NUMERICAL EXAMPLES

We now show some examples to illustrate the accuracy of the FORT method. We consider a vertical seismic profiling (VSP) configuration in which the source and the borehole are situated in a vertical plane (x, z). The borehole lies along the z-axis and the source is located on the surface ($z = 0$ km) at a distance of 1 km from the borehole. There are 24 receivers in the borehole separated by 40 m; the first receiver is at a depth of 40 m. We consider two types of models: one transversely isotropic (TI model) and one orthorhombic (ORTHO model). If we use a common measure of qP-wave anisotropy (maximum of $|\epsilon| \times 100\%$, where ϵ stands for ϵ_x, ϵ_y, or ϵ_z), the anisotropy of the qP-wave in the model TI is about 8%; in the ORTHO model it is about 20%. The anisotropy in the ORTHO model cannot be considered weak. Although the FORT method can accommodate arbitrary lateral variation of elastic moduli, the two models exhibit only vertical variation. Even in such models, calculated rays may exhibit 3D character. We specify the stiffness matrices at the top of the model (at $z = 0$ km) and at a certain depth z_{max}; then we interpolate the values of their elements linearly between the two levels. By varying z_{max}, we can vary the strength of the vertical gradient.

In the following, we measure the accuracy of the FORT method in the two types of models with varying gradients by plotting the relative time differences:

$$\frac{t_{FORT} - t_{exact}}{t_{exact}} \times 100\%. \tag{36}$$

The times t_{FORT} are obtained by the approach described in the preceding sections, i.e., by solving the FORT equations. The times t_{exact} are computed by a standard ray tracer for anisotropic media — a modified program package called ANRAY (Gajewski and Pšenčík, 1990). Two sets of relative time differences are shown in the following plots. One corresponds to the traveltimes provided directly by the FORT algorithm with first-order traveltimes; they are denoted by circles in the plots. The other is for the traveltimes corrected by the second-order term 33; they are denoted by crosses. To evaluate the second-order traveltime correction 33, it is necessary to specify the reference isotropic medium whose P- and S-wave velocities appear in equation 33. We use $V_S^2 = V_P^2/3$ and $V_P^2 = (p_k p_k)^{-1}$, where p_k are the components of the slowness vector obtained during the integration of the FORT system. The values of V_P and V_S determined in this way are used in all of the following computations because they are the specifications of V_P and V_S that yield the best results. Dependence of the results on the V_P/V_S ratio is negligible.

TI models

The density-normalized stiffness matrices of TI models with elements, measured in (kilometers/second^2), are

$$\begin{pmatrix} 15.71 & 5.05 & 4.46 & 0 & 0 & 0 \\ & 15.71 & 4.46 & 0 & 0 & 0 \\ & & 13.39 & 0 & 0 & 0 \\ & & & 4.98 & 0 & 0 \\ & & & & 4.98 & 0 \\ & & & & & 5.33 \end{pmatrix}$$

for the top of the models and

$$\begin{pmatrix} 35.35 & 11.36 & 10.04 & 0 & 0 & 0 \\ & 35.35 & 10.04 & 0 & 0 & 0 \\ & & 30.13 & 0 & 0 & 0 \\ & & & 11.21 & 0 & 0 \\ & & & & 11.21 & 0 \\ & & & & & 11.99 \end{pmatrix} \quad (37)$$

for the bottom of the models. We use Voigt notation in matrices 37. The variation of the qP-wave phase velocities in a vertical plane from a horizontal (0°) to a vertical (90°) direction of the wave normal are shown in Figure 1 for the top and the bottom of the model. Numerical experiments were performed for three specific models: HTI, ISO, and HTI-ROT, described below. The depth z_{max} of model 37 was 3 km.

Figure 2 shows the behavior of rays and traveltimes. Specifically, it shows projections of the exact 3D rays into the vertical plane containing the source and the borehole (bottom) into the horizontal plane (middle) and the traveltime curve (top) for the HTI-ROT model, The ray diagrams and traveltime curves are similar for the other considered models. Only the extent of deviation of rays from the vertical plane varies; therefore, we do not show them. Neither do we show the corresponding FORT-method plots because at the scales used in Figure 2, they coincide perfectly with the exact plots. To differentiate between the FORT and exact traveltimes, we plot their relative differences of equation 36 in Figures 3–5.

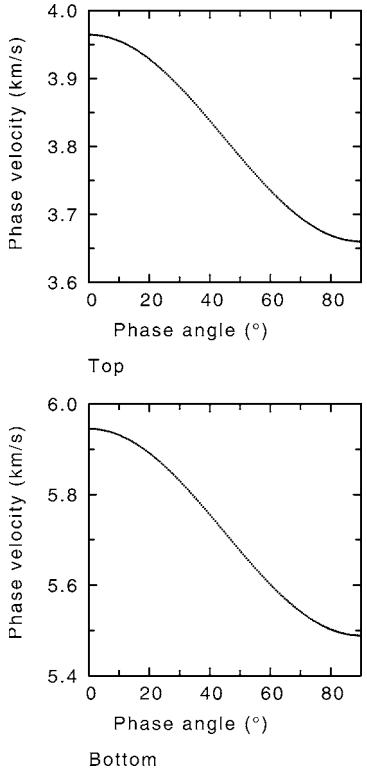

Figure 1. The qP-wave phase-velocity variations corresponding to stiffness matrices specified in equation 37 from horizontal (0°) to vertical (90°) direction of the wave normal. The upper plot corresponds to $z = 0$ km, the lower plot to $z = 3$ km.

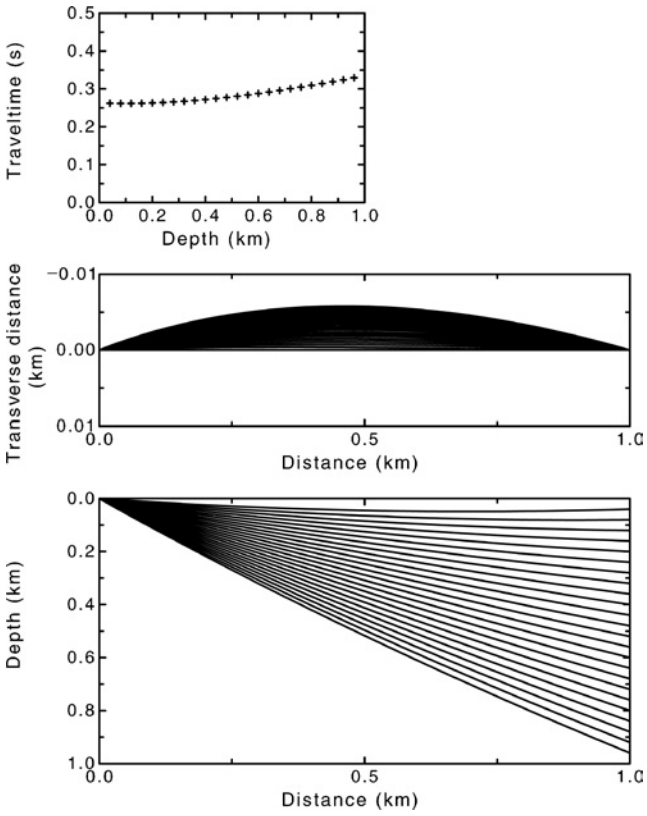

Figure 2. Projections of the ray diagram into the vertical plane containing the source and the borehole (bottom), into the horizontal plane (middle), and a traveltime curve (top) for the HTI-ROT model.

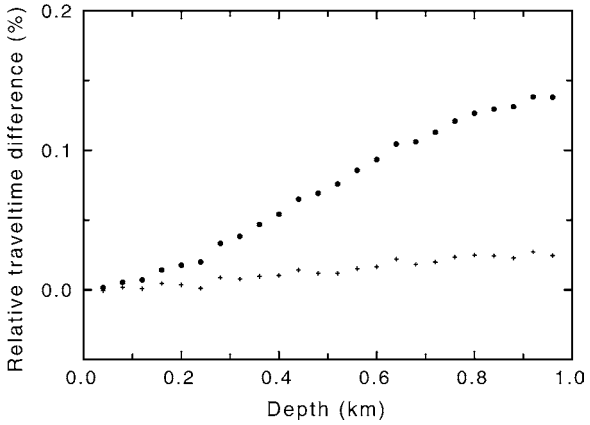

Figure 3. Relative traveltime differences of the first-order (traveltimes calculated along FORT rays — circles) and of the second-order (including traveltime correction 33 — crosses) approximations for the HTI model.

In Figure 3, the relative traveltime differences corresponding to the first- and second-order traveltimes are plotted for the HTI model. It is obtained from the model specified in equation 37 by rotating the axes of symmetry at the top and the bottom of the model so they are parallel to the x-axis, i.e., to the line connecting the source and the top of the borehole. Because the depth of the bottom of the model is considered to be at $z = 3$ km, the velocity gradient is rather strong — approximately 0.7 s^{-1}. In this case, the rays are confined to the (x, z) plane. We can see from Figure 3 that for rays terminating at shallow receivers, the accuracy of the first-order traveltimes is rather high — around 0.01%. This is numerical proof that the accuracy of the first-order phase velocity increases with decreasing deviation of the polarization vectors from the wave normal. For shallow receivers, the wave propagates close to the axis of symmetry, which is a longitudinal direction, along which the qP-wave normal and polarization vector are parallel and $B_{13} = B_{23} = 0$. A similar phenomenon can be observed for the VTI model, i.e., for the unrotated model (not presented here) specified in equation 37, because any direction perpendicular to the axis of symmetry of a TI medium is also a longitudinal direction for which $g_i = n_i$. With increasing receiver depth, the accuracy of the first-order traveltimes decreases, but their relative error never exceeds 0.15%.

If second-order traveltime correction 33 is used, the relative traveltime difference drops below approximately 0.03% for all considered receivers.

In Figure 4, the results for the ISO model are shown. The Iso model is obtained from the model given in equation 37 by orienting the axes of symmetry at the top and the bottom of the model perpendicularly to the vertical (x, z) plane containing the source and the borehole. The rays are again confined to the (x, z) plane, which now coincides with the plane of isotropy. We can see that the first-order traveltimes are obtained with high accuracy for all receivers. The differences are less than approximately 0.02%. The second-order correction is zero in this case because all directions in the (x, z) plane are longitudinal, for which B_{13} and B_{23} in equation 33 vanish.

Figure 5 shows relative traveltime differences for the HTI-ROT model. In this model, on the surface ($z = 0$ km) the axis of symmetry deviates by 45° from the x-axis in a horizontal plane. At the bottom of the model at a depth of $z = 3$ km, it is oriented along the x-axis. In between, as depth varies, the axis of symmetry smoothly rotates in a horizontal plane. Exact rays corresponding to this model are shown in Figure 2. We can see that they deviate slightly from the vertical plane. The first-order traveltime differences are practically the same for all receivers — slightly larger than 0.1%. Use of the second-order correction (equation 33) significantly reduces the error of the first-order traveltimes. The resulting difference does not exceed 0.05%. The errors increase slightly with depth.

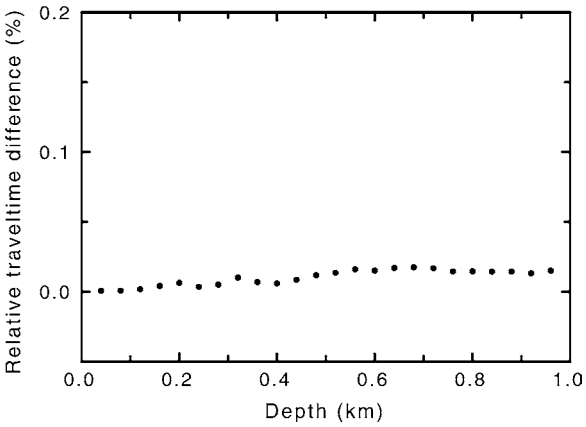

Figure 4. The same as in Figure 3 but for the ISO model.

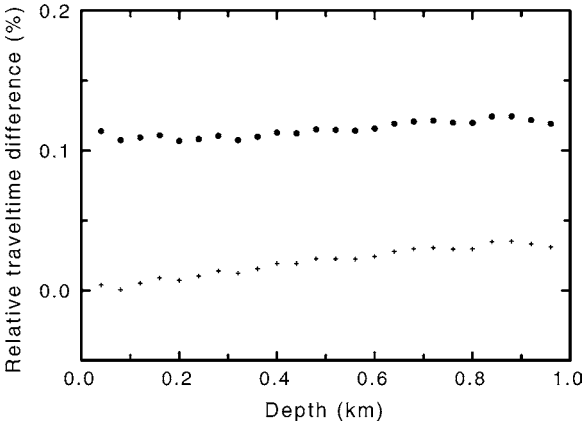

Figure 5. The same as in Figure 3 but for the HTI-ROT model.

ORTHO models

Let us now consider models based on the model of Schoenberg and Helbig (1997), which has anisotropy substantially larger than for the TI models previously considered (anisotropy is about 20%). The density-normalized stiffness matrices of the ORTHO models with elements measured in (kilometers/second) are

$$\begin{pmatrix} 9.00 & 3.60 & 2.25 & 0 & 0 & 0 \\ & 9.84 & 2.40 & 0 & 0 & 0 \\ & & 5.94 & 0 & 0 & 0 \\ & & & 2.00 & 0 & 0 \\ & & & & 1.60 & 0 \\ & & & & & 2.18 \end{pmatrix}$$

at the top and

$$\begin{pmatrix} 19.80 & 7.92 & 4.95 & 0 & 0 & 0 \\ & 21.65 & 5.28 & 0 & 0 & 0 \\ & & 13.07 & 0 & 0 & 0 \\ & & & 4.40 & 0 & 0 \\ & & & & 3.52 & 0 \\ & & & & & 4.80 \end{pmatrix} \tag{38}$$

at the bottom.

Variations of the qP-wave phase velocities in the vertical (x, z) plane (left column) and the vertical (y, z) plane (right

column) are shown in Figure 6 for a horizontal (0°) to a vertical (90°) direction of the wave normal for the top and the bottom of the model. Numerical experiments were performed for two specific models: ORT and ORT-ROT, described below. For presented results, the depth z_{max} of model 38 was 3 km.

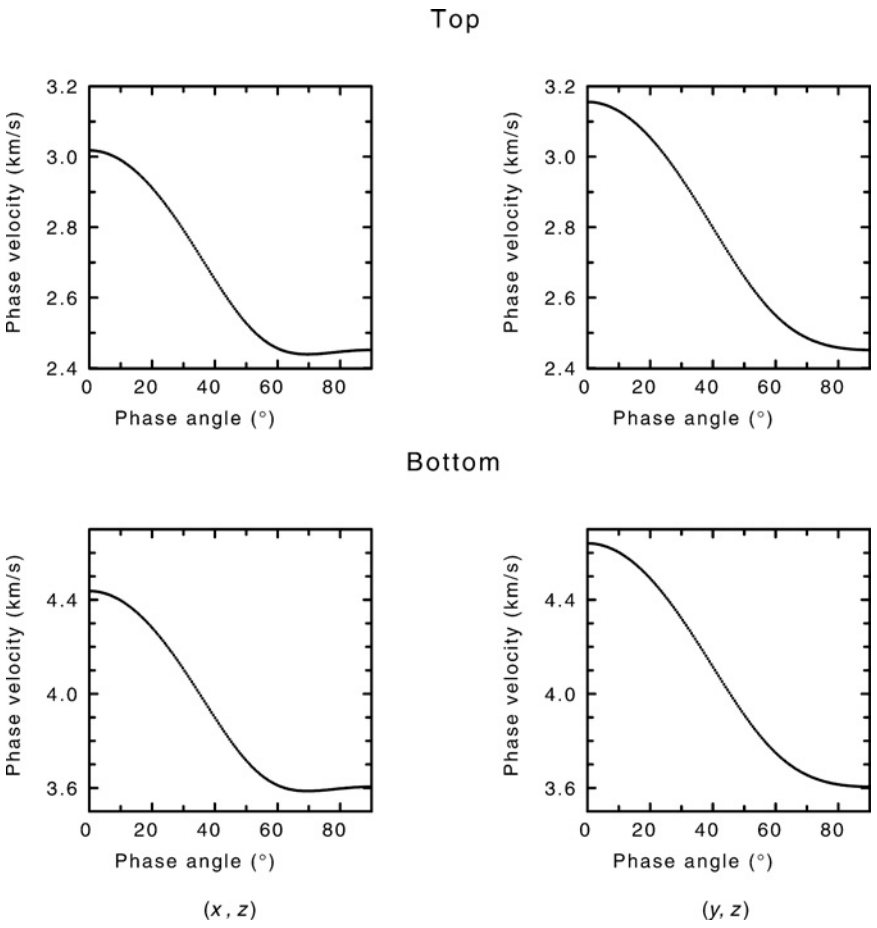

Figure 6. The qP-wave phase-velocity variations corresponding to stiffness matrices specified in equation 38 from the horizontal (0°) to the vertical (90°) direction of the wave normal. The upper plots correspond to $z = 0$ km, the lower plots to $z = 3$ km. The left column corresponds to the (x, z) plane, the right column to the (y, z) plane.

In Figure 7, relative differences of the traveltime in the first- and second-order approximation are shown for the (x, y) plane of the ORT model. Varying the vertical gradient in the model has negligible effects on the results. The traveltime differences may only increase in weakly inhomogeneous or homogeneous media in which rays are nearly straight. If such a straight ray is oriented in a direction in which the first-order approximation $G^{(1)}$ does not approximate well the eigenvalue G, the traveltime differences accumulate. In inhomogeneous media, rays curve and thus map onto varying directions; the traveltime errors associated with specific directions do not have a chance to accumulate. Traveltimes should thus be more accurate for inhomogeneous media.

Because of the stronger anisotropy, the maximum first-order traveltime difference slightly exceeds 1.5%. Application of the second-order correction (equation 33) substantially decreases the error. Except at several shallow receivers, the second-order corrected errors do not exceed 0.2%.

The character of curves in Figure 7 changes if we rotate differentially the stiffness matrices in equation 38. This is shown in Figure 8, which corresponds to the ORT-ROT model. In this model, the upper matrix of model 38 is first rotated by 45° around the z-axis; then the z-axis is rotated by 45° around the new y-axis. The bottom matrix of the model ORT-ROT, corresponding to a depth of $z = 3$ km, is not rotated. The first-order differences are always less than 1% in this

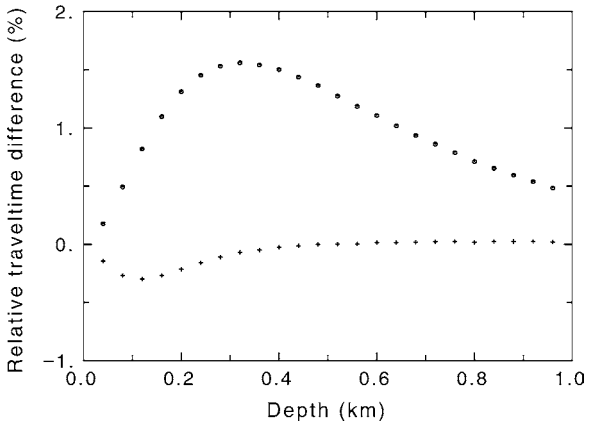

Figure 7. Relative traveltime differences of the first-order (traveltimes calculated along FORT rays — circles) and of the second-order (including traveltime correction 33 — crosses) approximations for the ORT model.

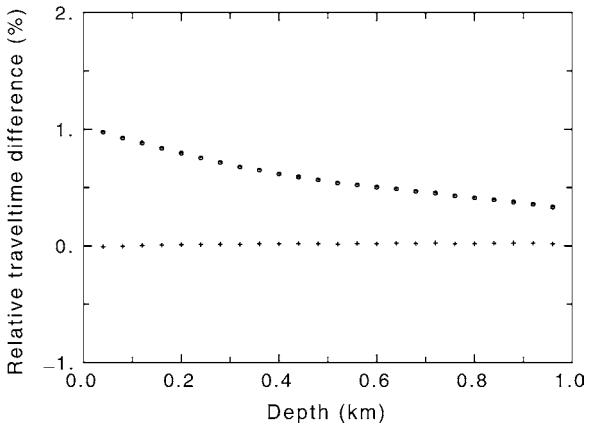

Figure 8. The same as in Figure 7 but for the ORT-ROT model.

model. Applying the second-order correction term of equation 33 leads to effectively zero errors.

CONCLUSIONS

The FORT and FODRT equations for qP-waves propagating in inhomogeneous weakly anisotropic media have several important and interesting properties. They are expressed in terms of the weak-anisotropy parameters, which represent a more natural description of a weakly anisotropic medium than standard elastic moduli. The qP-wave FORT equations have a simpler and more transparent form than the exact ray-tracing equations. In the most general case, they depend only on the 15 qP-wave weak-anisotropy parameters. The FORT equations allow qP-waves to be treated independently from qS-waves, just as in isotropic media. The FORT equations can thus substitute for traditional isotropic ray tracers in many routine applications such as prestack Kirchhoff depth migration. They can be used both in ray tracing and in wavefront construction codes. Because of the simplicity of FORT equations, they are computationally more effective than standard ray-tracing equations. FORT equations are universal for inhomogeneous isotropic and anisotropic media. In isotropic media they yield exact rays; in anisotropic media, their first-order approximations.

In contrast to other perturbation techniques used to trace rays in weakly anisotropic media, our approach does not require calculation of reference rays in a reference isotropic medium. The FORT-method rays are obtained directly. A reference medium is required only for calculating the second-order traveltime correction. As mentioned earlier, the best results are obtained if the qP-wave reference velocities are determined from the relevant slowness vectors obtained from the FORT method.

The use of the FORT method with second-order traveltime corrections results in traveltime errors that are effectively negligible even for media with anisotropy of 20%. Our tests indicate only a very weak dependence of the effectiveness of the FORT method on the strength of the inhomogeneity of the medium. As expected, the accuracy depends mostly on the strength of the anisotropy being considered instead of on its type. The decisive factor for accuracy of the first-order (second-order) traveltime computations is the accuracy of approximating the exact polarization vectors by their zero-order (first-order) approximations.

First-order dynamic ray tracing offers the same broad variety of applications as its exact counterpart. Because FODRT represents a system of linear differential equations, it can be solved using propagator techniques just as for traditional dynamic ray tracing.

The next planned steps in this study are to use the FODRT method to solve for geometrical spreading and to generalize the approach to layered media. This will allow calculation of synthetic seismograms using the FORT and FODRT equations in laterally varying layered isotropic and anisotropic media. Further extensions are directed toward qS-waves.

ACKNOWLEDGMENTS

The authors are greatly indebted to Sláva Červený, Pat Daley, Joe Dellinger, Petr Jílek, and Einar Iversen for their critical and constructive reviews. This work was supported by the CNRS-AS ČR project, the Seismic Waves in Complex 3-D Structures (SW3D) consortium project, research project A3012309 of the Grant Agency of the Academy of Sciences of the Czech Republic, and research projects Z3012916 and K3012103 of the Academy of Sciences of the Czech Republic.

APPENDIX A

qP-WAVE WEAK-ANISOTROPY PARAMETERS AND EXPRESSIONS FOR B_{13}, B_{23}, AND B_{33}

If we denote by α the P-wave velocity of a reference isotropic medium, we can introduce 15 qP-wave weak-anisotropy parameters in the following way:

$$\begin{aligned}
&\epsilon_x = \frac{A_{11}-\alpha^2}{2\alpha^2}, \quad \epsilon_y = \frac{A_{22}-\alpha^2}{2\alpha^2}, \quad \epsilon_z = \frac{A_{33}-\alpha^2}{2\alpha^2},\\
&\delta_x = \frac{A_{13}+2A_{55}-\alpha^2}{\alpha^2}, \quad \delta_y = \frac{A_{23}+2A_{44}-\alpha^2}{\alpha^2},\\
&\delta_z = \frac{A_{12}+2A_{66}-\alpha^2}{\alpha^2}, \quad \chi_x = \frac{A_{14}+2A_{56}}{\alpha^2},\\
&\chi_y = \frac{A_{25}+2A_{46}}{\alpha^2}, \quad \chi_z = \frac{A_{36}+2A_{45}}{\alpha^2},\\
&\epsilon_{15} = \frac{A_{15}}{\alpha^2}, \quad \epsilon_{16} = \frac{A_{16}}{\alpha^2}, \quad \epsilon_{24} = \frac{A_{24}}{\alpha^2},\\
&\epsilon_{26} = \frac{A_{26}}{\alpha^2}, \quad \epsilon_{34} = \frac{A_{34}}{\alpha^2}, \quad \epsilon_{35} = \frac{A_{35}}{\alpha^2}.
\end{aligned} \tag{A-1}$$

Here, $A_{\alpha\beta}$ are the density-normalized elastic moduli in Voigt notation.

The elements B_{13}, B_{23}, and B_{33} of matrix B_{mn} (see equation 32), important for qP-wave studies, can be expressed explicity in the following way:

$$\begin{aligned}
B_{13} = {} & \alpha^2 D^{-1}\{n_3^4(\epsilon_{34}n_2+\epsilon_{35}n_1)+n_3^3[\eta_y n_1^2\\
& +\eta_x n_2^2+2\chi_z n_1 n_2]\\
& +n_3^2[(4\chi_x-3\epsilon_{34})n_1^2 n_2+(4\chi_y-3\epsilon_{35})n_1 n_2^2\\
& +(4\epsilon_{15}-3\epsilon_{35})n_1^3+(4\epsilon_{24}-3\epsilon_{34})n_2^3]\\
& +n_3[(2\eta_z-\eta_x-\eta_y)n_1^2 n_2^2+2(2\epsilon_{16}-\chi_z)n_1^3 n_2\\
& +2(2\epsilon_{26}-\chi_z)n_1 n_2^3\\
& -\eta_y n_1^4-\eta_x n_2^4+(\epsilon_x-\epsilon_z)n_1^2\\
& +(\epsilon_y-\epsilon_z)n_2^2]-\chi_x n_1^2 n_2-\chi_y n_1 n_2^2\\
& -\epsilon_{15}n_1^3-\epsilon_{24}n_2^3\},\\
B_{23} = {} & \alpha^2 D^{-1}\{n_3^3(\epsilon_{34}n_1-\epsilon_{35}n_2)\\
& +n_3^2[(\eta_x-\eta_y)n_1 n_2+\chi_z n_1^2-\chi_z n_2^2]\\
& +n_3[(2\chi_y-3\epsilon_{15})n_1^2 n_2\\
& -(2\chi_x-3\epsilon_{24})n_1 n_2^2+\chi_x n_1^3-\chi_y n_2^3]\\
& +\eta_z n_1^3 n_2-\eta_z n_1 n_2^3+3(\epsilon_{26}-\epsilon_{16})n_1^2 n_2^2\\
& +\epsilon_{16}n_1^4-\epsilon_{26}n_2^4+(\epsilon_y-\epsilon_x)n_1 n_2\},
\end{aligned}$$

$$B_{33} = \alpha^2 + 2\alpha^2\{(\epsilon_x n_1^2 + \epsilon_y n_2^2 + \epsilon_z n_3^2) + (\eta_x n_2^2 n_3^2 + \eta_y n_3^2 n_1^2 + \eta_z n_1^2 n_2^2) + 2[(\epsilon_{16} n_2 + \epsilon_{15} n_3) n_1^3 + (\epsilon_{24} n_3 + \epsilon_{26} n_1) n_2^3 + (\epsilon_{35} n_1 + \epsilon_{34} n_2) n_3^3 + (\chi_x n_1 + \chi_y n_2 + \chi_z n_3) n_1 n_2 n_3]\}. \quad \text{(A-2)}$$

For η_x, η_y, and η_z, see equation 13. Expressions A-2 correspond to the following choice of vectors $\mathbf{e}^i$ in equation 32:

$$\begin{aligned} \mathbf{e}^1 &\equiv D^{-1}(n_1 n_3, n_2 n_3, n_3^2 - 1), \\ \mathbf{e}^2 &\equiv D^{-1}(-n_2, n_1, 0), \\ \mathbf{e}^3 &= n_i \equiv (n_1, n_2, n_3), \end{aligned} \quad \text{(A-3)}$$

where

$$D = (n_1^2 + n_2^2)^{1/2}, \qquad n_1^2 + n_2^2 + n_3^2 = 1. \quad \text{(A-4)}$$

The symbol n_i denotes a unit normal to the wavefront.

As mentioned in the text after equation 32, $G^{(1)} = B_{33}$, i.e., the expressions for B_{33} in equation A-2 and for G in equation 12 are identical. If density-normalized elastic moduli $A_{\alpha\beta}$ are used instead of weak-anisotropy parameters, B_{33} and $G^{(1)}$ can be rewritten in the following form:

$$G^{(1)} = B_{33} = A_{11} n_1^2 + A_{22} n_2^2 + A_{33} n_3^2 + E_x n_2^2 n_3^2 + E_y n_3^2 n_1^2 + E_z n_1^2 n_2^2 + 4[(C_x n_1 + C_y n_2 + C_z n_3) n_1 n_2 n_3 + (A_{16} n_2 + A_{15} n_3) n_1^3 + (A_{24} n_3 + A_{26} n_1) n_2^3 + (A_{35} n_1 + A_{34} n_2) n_3^3]. \quad \text{(A-5)}$$

Here,

$$\begin{aligned} E_x &= 2A_{23} + 4A_{44} - A_{22} - A_{33}, \\ E_y &= 2A_{13} + 4A_{55} - A_{11} - A_{33}, \\ E_z &= 2A_{12} + 4A_{66} - A_{11} - A_{22}, \\ C_x &= A_{14} + 2A_{56}, \\ C_y &= A_{25} + 2A_{46}, \quad C_z = A_{36} + 2A_{45}. \end{aligned} \quad \text{(A-6)}$$

Note that expression A-5 for B_{33} is completely independent of α. Similar expressions, also independent of α, could be written for B_{13} and B_{23}. Again, α appears in equation A-2 only as a consequence of our use of the weak-anisotropy parameters A-1.

REFERENCES

Červený, V., 2001, Seismic ray theory: Cambridge University Press.

Daley, P. F., K. J. Marfurt, and E. B. McCarron, 1999, Finite-element ray tracing through structurally deformed transversely isotropic formations: Geophysics, **64**, 954–962.

Farra, V., 1989, Ray perturbation theory for heterogeneous hexagonal anisotropic medium: Geophysical Journal International, **99**, 723–738.

———, 2001, High order expressions of the phase velocity and polarization of qP and qS waves in anisotropic media: Geophysical Journal International, **147**, 93–105.

———, 2004, Improved first-order approximation of group velocities in weakly anisotropic media: Studia Geophysica et Geodetica, **48**, 199–213.

———, 2005, First-order ray tracing for qS waves in inhomogeneous weakly anisotropic media: Geophysical Journal International, **161**, 309–324.

Farra, V., and S. LeBégat, 1995, Sensitivity of qP-wave travel times and polarization vectors to heterogeneity, anisotropy and interfaces: Geophysical Journal International, **121**, 371–384.

Farra, V., and I. Pšenčík, 2003, Properties of the zero-, first- and higher-order approximations of attributes of elastic waves in weakly anisotropic media: Journal of the Acoustic Society of America, **114**, 1366–1378.

Gajewski, D., and I. Pšenčík, 1990, Vertical seismic profile synthetics by dynamic ray tracing in laterally varying layered anisotropic structures: Journal of Geophysical Research, **95**, 11301–11315.

Nowack, R. L., and I. Pšenčík, 1991, Perturbation from isotropic to anisotropic heterogeneous media: Geophysical Journal International, **106**, 1–10.

Portugal, R., A. Aggio, and E. Filpo, 2003, Wavefront construction in a weakly anisotropic medium using isotropic ray tracing with velocity perturbation: 8th Congress, Sociedade Brasileira de Geofisica, Expanded Abstracts, 460.

Pšenčík, I., and V. Vavryčuk, 2002, Approximate relation between the ray vector and the wave normal in weakly anisotropic media: Studia Geophysica et Geodetica, **46**, 793–807.

Schoenberg, M., and K. Helbig, 1997, Orthorhombic media: Modeling elastic wave behavior in a vertically fractured earth: Geophysics, **62**, 1954–1974.

Thomsen, L., 1986, Weak elastic anisotropy: Geophysics, **51**, 1954–1966.

Vinje, V., E. Iversen, and H. Gjoystdal, 1993, Traveltime and amplitude estimation using wavefront construction: Geophysics, **58**, 1157–1166.